O. Labban, T. Chen, A.F. Ghoniem, J.H. Lienhard V, and L.K. Norford, "Next-Generation HVAC: Prospects for and Limitations of Desiccant and Membrane-Based Dehumidification and Cooling," *Applied Energy*, **200**:330–346, 15 August 2017.

Next-generation HVAC: Prospects for and limitations of desiccant and membrane-based dehumidification and cooling

Omar Labban,[†,¶] Tianyi Chen,[†,¶] Ahmed F. Ghoniem,[†,§] John H. Lienhard V,[†,§] and Leslie K. Norford[*,‡,§]

†*Department of Mechanical Engineering, Massachusetts Institute of Technology, Cambridge, United States*

‡*Department of Architecture, Massachusetts Institute of Technology, Cambridge, United States*

¶*Joint first authors.*

§*Joint senior authors.*

E-mail: lnorford@mit.edu

Abstract

Recently, next-generation HVAC technologies have gained attention as potential alternatives to the conventional vapor-compression system (VCS) for dehumidification and cooling. Previous studies have primarily focused on analyzing a specific technology or its application to a particular climate. A comparison of these technologies is necessary to elucidate the reasons and conditions under which one technology might outperform the rest. In this study, we apply a uniform framework based on fundamental thermodynamic principles to assess and compare different HVAC technologies from

*Corresponding author.

an energy conversion standpoint. The thermodynamic least work of dehumidification and cooling is formally defined as a thermodynamic benchmark, while VCS performance is chosen as the industry benchmark against which other technologies, namely desiccant-based cooling system (DCS) and membrane-based cooling system (MCS), are compared. The effect of outdoor temperature and humidity on device performance is investigated, and key insights underlying the dehumidification and cooling process are elucidated. In spite of the great potential of DCS and MCS technologies, our results underscore the need for improved system-level design and integration if DCS or MCS are to compete with VCS. Our findings have significant implications for the design and operation of next-generation HVAC technologies and shed light on potential avenues to achieve higher efficiencies in dehumidification and cooling applications.

Keywords

Next-generation HVAC, Dehumidification, Thermodynamic least work, Vapor-compression, Desiccants, Membranes

Nomenclature

Roman symbols

c_p	specific heat at constant pressure, kJ/(kg · K)
COP	coefficient of performance
h	specific enthalpy, kJ/kg dry air
h_{fg}	enthalpy of vaporization, kJ/kg
$\dot{m}$	mass flow rate of dry air, kg/s
$\dot{Q}$	rate of heat transfer, kW
P	pressure, kPa
r_p	compression ratio
R_a	ideal gas constant of dry air, 0.287 kJ/(kg · K)
RH	relative humidity
s	specific entropy, kJ/(K · kg dry air)
$\dot{S}_{gen}$	rate of entropy generation, kW/K
T	temperature, K
$\dot{W}$	rate of work transfer, kW
$\dot{w}$	specific work transfer, kJ/kg dry air

Greek symbols

α	humidity removal fraction
η_{II}	second law efficiency
ϵ_{HX}	heat exchanger effectiveness
ϵ_S	membrane exchanger sensible effectiveness
ϵ_L	membrane exchanger latent effectiveness
ω	humidity ratio, kg moisture/kg dry air
$\tilde{\omega}$	mole fraction of vapor to air in the moist air mixture

ξ	total specific exergy, kJ/kg dry air

Subscripts

a	dry air
ad	adsorption
c	cooling
$cool$	cooling load
$coil$	cooling coil
$cond$	condensation
h	heating
i	stream identity
lat	latent load
p	pressure
reg	regeneration
sat	saturation
v	vapor
w	liquid water
0	environment or dead state

Abbreviations

DCS	desiccant-based cooling system
DW	desiccant wheel
IEC	indirect evaporative cooler
MCS	membrane-based cooling system
VCS	vapor-compression system

1 Introduction

Building operation consumes more than 40 percent of the total energy used in the United States,[1] and building heating and cooling loads comprise the largest fraction. Demand for cooling energy is exacerbated in hot and humid climates. High humidity poses a serious limitation to the design and operation of buildings, promoting mold and dust mites and often associated with increased disease transmission. Consequently, dehumidifying air in building ventilation systems is normally a requirement to mitigate the effects of high humidity, improve indoor thermal comfort, and meet indoor design conditions.

For over a century, the vapor-compression system (VCS) has been the de facto technology of choice in heating, ventilation, and air conditioning (HVAC), especially for dehumidification and cooling. In spite of its success, research, policy, and economics all encourage change in light of its many inherent shortcomings. From an energy standpoint, the inability of the VCS system to decouple latent and sensible loads leaves condensation, an energy intensive process, as the only means for dehumidification. The heart of the VCS system lies in the refrigerant, whose chemistry has evolved in response to policy and environmental concerns. From chlorofluorocarbons (CFCs) and hydrochlorofluorocarbons (HCFCs), banned under the Montreal Protocol in 1987,[2] to hydrofluorocarbons (HFCs), such as R-134a with a global warming potential (GWP) 1430 times that of carbon dioxide (CO_2),[3] environmental concerns associated with VCS can no longer be overlooked. These concerns, coupled with potential excess greenhouse gas (GHG) emissions resulting from the inefficiencies inherent in the system, place research on future HVAC technologies at the cornerstone of any effort aimed at mitigating climate change.

The United States, Canada, and Mexico recently proposed to curb their use of HFCs by 85% between 2016–2033,[4] while several members of the European Union supported an agreement to phase out HFCs by 80% between 2016–2030.[5] These efforts, among others, paved the way for the Kigali accord, an amendment to the Montreal Protocol signed by more than 170 countries to phase out HFCs. In response to the rising interest in the future

of HVAC, Chua et al.[6] presented a review of recent HVAC innovations to achieve improved air-conditioning efficiency, while the U.S. DOE published a study shortlisting potential next-generation HVAC technologies,[7,8] highlighting the potential of two technologies of interest to our study, desiccant and membrane technologies.

Desiccant technology employs desiccants, normally solid or liquid materials with a high affinity for water vapor, to separate water vapor from outdoor air and thereby decouple dehumidification from the cooling process.[9] Daou et al.[10] reviewed different configurations of the desiccant cooling system (DCS), and La et al.[11] pointed out the merits of the solid rotary DCS (known as a desiccant wheel): compactness, continuous working hours, and lower susceptibility to corrosion during operation. To analyze its potential for regeneration using low-grade heat, Angrisani et al.[12,13] experimentally investigated the effect of outdoor conditions and regeneration temperature on desiccant wheel performance. Given the promise desiccants offer for more efficient air conditioning, several configurations employing desiccant wheels, such as the combined chilled-ceiling desiccant cooling system,[14] continue to be investigated in the literature.

In contrast with desiccant technology, the isothermal nature of chemical separation in membrane technology poses a unique advantage, and its incorporation in HVAC has lately been an active field of research. In recent reviews, Woods[15] and Zhang[16] provided overviews of the latest membrane developments in HVAC and a summary of potential avenues for future research, while another review by Yang et al.[17] highlighted the major advances membrane technology has made in air dehumidification. In search of membranes with the greater selectivity necessary to make this process viable, Zhang et al.[18] developed a novel membrane using a polyethersulfone (PES) support layer coupled with a polyvinylalcohol (PVA) active layer, while Bui et al.[19,20] later reported the fabrication of a robust hydrophilic PVA/LiCl composite membrane. Other studies explored boosting air-conditioning performance through incorporating membrane-based total heat recovery,[21,22] enabling heat and mass exchange across air streams.

Another prominent application of membrane technology has been membrane-based liquid desiccant dehumidification, recently reviewed by Huang et al.[23] and Abdel-Salam et al.[24] Compared to solid desiccants, liquid desiccants allow for localized dehumidification and for regeneration to occur at lower temperatures,[9] while integrating them with membranes eliminates the challenge of desiccant cross-over.[23] Research in the field continues to investigate several aspects of this technology, including modeling system performance,[25–27] improving system design,[28] and employing renewable energy.[29]

Apart from the question of which technology produces the dehumidification and cooling effect, HVAC is an energy conversion process, whose design and performance can considerably benefit from a greater thermodynamic understanding. Even many decades after the inception of VCS, for example, thermodynamic analysis aimed at improving VCS performance and efficiency continues to be relevant to this day, as evident from the works of Kumar et al.,[30] Bayrakçi and Özgür,[31] and a recent review by Ahamed et al.,[32] to name a few. Similarly, Zhang[33] presented an energy analysis of several air dehumidification systems, Sakulpipatsin et al.[34] applied energy and exergy analysis to buildings and HVAC systems, while Qureshi and Zubair[35] applied them to analyze various psychrometric processes, and Caliskan et al.[36] extended the analysis to assess the performance of the novel Maisotsenko cycle (M-Cycle). In addition, energy analysis for a desiccant wheel (DW) has been performed by Mohsen et al.,[37] while a recent work by Bynum[38] explored the thermodynamic modeling of a membrane-based dehumidification system.

While significant progress continues to be made in the area of energy/exergy analysis and next-generation HVAC technologies, a broader impact study comparing the advantages and limitations of each technology, while bringing about further insights into the dehumidification and cooling process, has been missing in the literature. In spite of the advancements made thus far, our understanding of how these technologies perform relative to a thermodynamic benchmark (a step necessary to gauge the current status of the technology), how each technology fares relative to competitors, and how much room is left for improvement,

has been limited. Similarly, an investigation into the effect of climate conditions on system performance and the implications of such an effort on technology adoption under different climates is still needed. In spite of the significant improvements that dehumidification and cooling technologies could potentially achieve through careful system design, integration, and energy recuperation, as our study demonstrates, studies in the literature have mainly focused on either one system configuration or on multiple commercially existing ones.

Our work presents an evaluation of different HVAC technologies from the standpoint of energy conversion. A framework based on fundamental thermodynamic principles is developed to define a thermodynamic benchmark in terms of the least work and to assess the potential of the DCS and the MCS compared to the conventional VCS, while uncovering the prospects and limitations of each technology. Unlike previous studies, different technologies are compared against each other, the effect of climate conditions on technology adoption is explored, and insights underlying a technology's superior performance under specific climate conditions are emphasized. As these technologies can be hybridized or integrated with other recuperation devices, we propose two approaches for evaluation: one aimed at the technologies themselves, and the other built on the developed insights to achieve more efficient system-design and integration. Our results demonstrate the great potential of the DCS and the MCS in dehumidification and cooling and reflect the dramatic impact of system-design and integration on system efficiency.

2 Thermodynamic least work of dehumidification and cooling

Before exploring the thermodynamics and energy costs associated with the different technologies, the thermodynamic least work, an overall benchmark, needs to be set up. This benchmark defines an idealized performance for dehumidification and cooling and gives insight into the loss mechanisms limiting the energy efficiency of real systems. In this section,

we start by defining a generalized dehumidification and cooling unit, then derive an expression for the thermodynamic least work of dehumidification and cooling, and close by conducting parametric studies to evaluate how the least work varies under different outdoor conditions.

2.1 Generalized dehumidification and cooling unit

To arrive at an expression for the thermodynamic least work of dehumidification and cooling, we begin by considering a typical ventilation system, depicted in Fig. 1. Outdoor air at a predefined state 1 (dependent on the geographical location/time of the year) and a flow rate (the lower bound of which is dictated by ASHRAE Standard 62.1[39] to satisfy indoor air quality requirements) enters the reversible/ideal dehumidification and cooling unit, and is processed to the prescribed supply conditions given by state 3. To simplify the analysis, we focus our attention in this study on the cooling loads associated with the outdoor ventilation air under the assumption that a separate system is employed to handle the indoor cooling loads. As Fig. 1 illustrates, the reversible dehumidification and cooling unit introduced may later be swapped for any of the three technologies of interest to this study without loss of consistency.

In addition to the processed stream, another interesting aspect of this separation process is the waste stream given by state 2 in Fig. 1. Depending on the technology we encounter later, minimizing the work input requires the separated moisture to leave the system at ambient conditions either in pure liquid form or as a saturated air/vapor mixture. Both cases will be considered in this derivation, allowing us to later invoke the appropriate definition based on the state of the waste stream (pure water or air/vapor mixture) generated for any given technology. Since the least work is defined under isothermal and isobaric conditions, the thermodynamic properties at state 2 are fixed for each case.

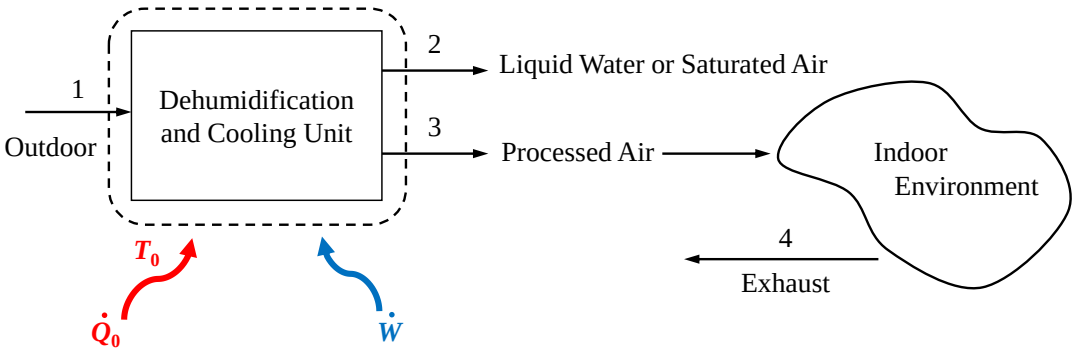

Figure 1: Control volume (dotted line) around dehumidification and cooling systems for least work calculation.

2.2 Theoretical derivation of the least work

Following our definition of the generalized dehumidification and cooling unit, we start the least work derivation by drawing a control volume around this unit, and allowing it to interact with the environment, as shown in Fig. 1. By combining the steady state first and second laws of thermodynamics, the rate of work transfer $\dot{W}$, following the positive work input sign convention, can be expressed as:[40]

$$\dot{W} = \dot{m}_2\xi_2 + \dot{m}_3\xi_3 - \dot{m}_1\xi_1 - \dot{Q}\left(1 - \frac{T_0}{T}\right) + T_0\dot{S}_{gen} \tag{1}$$

where ξ is the specific total exergy of the i^{th} stream, T is the temperature at which the heat transfer at a rate $\dot{Q}$ enters the system, $\dot{S}_{gen}$ refers to the rate of entropy generation in the system, $\dot{m}_i$ indicates the mass flow rate of dry air or condensed water, and the subscript 0 refers to the environment condition (or dead state).

Following the classical framework of modeling humid air as an ideal gas mixture, the total exergy of humid air per kilogram of dry air is evaluated following the relation:[41]

$$\xi = (c_{p,a} + \omega c_{p,v})T_0\left(\frac{T}{T_0} - 1 - \ln\frac{T}{T_0}\right) + (1+\tilde{\omega})R_aT_0\ln\frac{P}{P_0} + R_aT_0\left((1+\tilde{\omega})\ln\frac{1+\tilde{\omega}_0}{1+\tilde{\omega}} + \tilde{\omega}\ln\frac{\tilde{\omega}}{\tilde{\omega}_0}\right) \tag{2}$$

where $c_{p,a}$ and $c_{p,v}$ are the specific heat of air and vapor at a constant pressure P, ω the

humidity ratio, $\tilde{\omega}$ the mole fraction of vapor to air in the mixture, and R_a the ideal gas constant of dry air. Similarly, the specific total exergy of condensed water, a pure substance, is evaluated as:[41]

$$\xi = h_w(T, P) - h_0(T_0, P_{0,w}) - T_0 s_w(T, P) + T_0 s_0(T_0, P_{0,w}) \tag{3}$$

where h and s are the enthalpy and entropy of water evaluated at a given temperature and pressure, and $P_{0,w}$ is the vapor partial pressure at ambient conditions, computed as:[41]

$$P_{0,w} = \left(\frac{\tilde{\omega}_0}{1 + \tilde{\omega}_0}\right) P_0 \tag{4}$$

The minimum work is defined as the work input in a reversible process with no entropy generation, which corresponds to a thermodynamically ideal process. If no external heat source or sink (other than the environment) is assumed to exchange heat with the system,[40] the least work can then be expressed as:

$$\dot{W}_{min} = \dot{m}_2 \xi_2 + \dot{m}_3 \xi_3 - \dot{m}_1 \xi_1 \tag{5}$$

The mass conservation of dry air implies:

$$\begin{aligned} \dot{m}_1 &= \dot{m}_2 + \dot{m}_3 \quad \text{(If state 2 is a saturated air/vapor mixture)} \\ \dot{m}_1 &= \dot{m}_3 \quad \text{(If state 2 is condensed water)} \end{aligned} \tag{6}$$

Similarly, the conservation of water mass implies:

$$\begin{aligned} \dot{m}_1 \omega_1 &= \dot{m}_2 \omega_2 + \dot{m}_3 \omega_3 \quad \text{(If state 2 is a saturated air/vapor mixture)} \\ \dot{m}_1 \omega_1 &= \dot{m}_2 + \dot{m}_3 \omega_3 = \dot{m}_w + \dot{m}_3 \omega_3 \quad \text{(If state 2 is condensed water)} \end{aligned} \tag{7}$$

Here $\dot{m}_w$ is the mass flow rate of liquid water.

Due to the irreversibility of the thermodynamic process, the actual work input will always be larger than the least work and thus a second-law efficiency is defined to measure the relative performance of a given system compared to the ideal system:

$$\eta_{II} = \frac{\dot{W}_{min}}{\dot{W}_{actual}} \tag{8}$$

A different efficiency, the Coefficient of Performance (COP), is commonly used in HVAC systems to measure the ratio of useful cooling provided to the actual work input on a system.

$$\text{COP} = \frac{\dot{Q}}{\dot{W}} = \frac{\dot{m}_3(h_1 - h_3)}{\dot{W}_{actual}} \tag{9}$$

In this definition, $\dot{Q}$ refers to the sensible and latent heat removed from the outdoor air, and $\dot{W}$ refers to the corresponding actual work input.

2.3 Modeling results

The indoor air temperature is set as 24 °C in the following analysis, and the relative humidity is set to 50% since lower values may cause dry skin issues and higher ones may promote mold and bacteria growth.[37] To investigate the effect of outdoor conditions on performance, a parametric study has been performed with varying outdoor temperature and relative humidity, with a range of 24–53 °C in temperature and 50–95% in relative humidity.

As is shown in Fig. 2, the least work increases with rising outdoor temperature. At the same time, air with higher dry bulb temperature can absorb more water vapor, which increases the work to separate water vapor from the mixture. This rise is even more pronounced with increasing relative humidity. As our results demonstrate, the overall least work for the dehumidification and cooling process is below 13 kJ/kg dry air, and in normally hot days, the least work is under 5 kJ/kg dry air for both scenarios in state 2, which agrees with results reported by previous researchers.[42] The least work featuring a condensed waste stream in state 2 always exceeded that featuring a saturated air/vapor waste stream.

The difference between these two processes, however, did not exceed 25%, and diminished considerably with rising humidity.

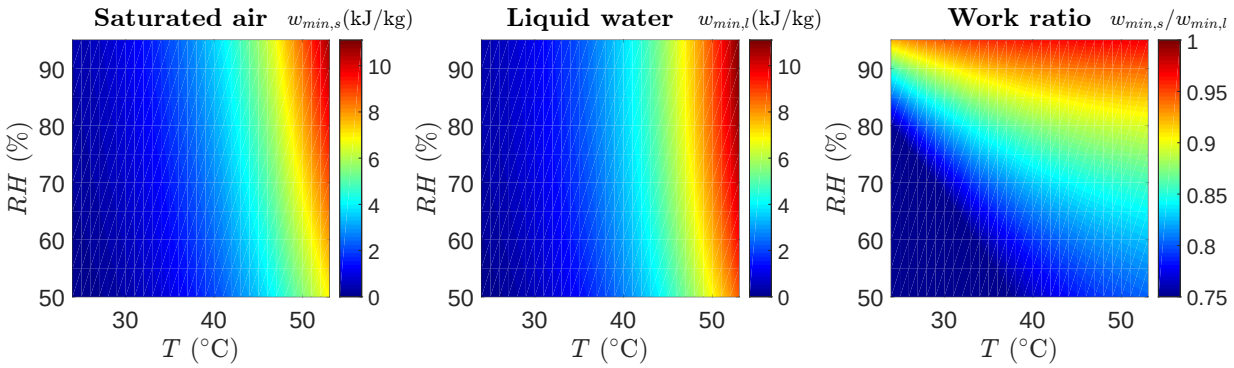

Figure 2: Least work for outdoor air conditions.

3 Energy analysis for VCS

In addition to the least work analysis presented, analyzing the performance of the VCS sets an industry benchmark against which the merits of other technologies can be assessed. This section starts by adopting the industry standard VCS with a traditional cooling coil to achieve the desired dehumidification and cooling effect. A thermodynamic model is developed, and parametric studies are run to quantify the limitations of this technology and unveil potential avenues for improvement.

3.1 Thermodynamic model of VCS

Figure 3 depicts a VCS with a traditional cooling coil, conditioning an indoor space.[43] To lower the energy consumption, a hot and humid outdoor air stream exchanges heat with return air before being passed through the cooling coil to reach the dew point temperature. At this point, water vapor starts condensing as the process follows the saturation line on the psychrometric chart until the desired humidity is reached. From there, the supply air is usually cold, and requires further conditioning to supply air to the room at the stated

conditions.

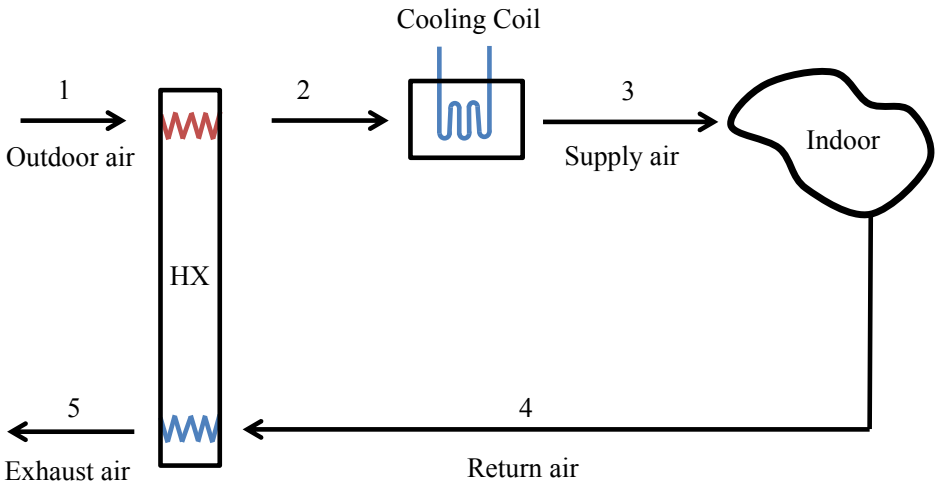

Figure 3: VCS with heat recovery.

This VCS process has the inherent limitation of not separating latent and sensible loads and requires unnecessary sensible cooling to lower the dew point of the supply air to the design value. Given our interest in supplying air at a particular design condition, we refrain from rewarding the system for supplying air that is cooler than necessary although a portion of this overcooling energy could be recuperated by mixing with indoor air. Likewise, we neglect any energy penalty associated with increasing the dry bulb temperature of the supply air to the design condition under the assumption that it is either unnecessary or that the ambient environment could be employed.

Developing a thermodynamic model for this system requires applying mass and energy balances to a control volume encompassing the cooling coil to arrive at:

$$\dot{m}_w = \dot{m}_2(\omega_2 - \omega_3) \tag{10}$$

$$\dot{Q} = \dot{m}_2(h_2 - h_3) - \dot{m}_w h_w \tag{11}$$

The second term is usually small relative to the first term on the right of Eq. 11, and may

reasonably be neglected.[43] The cooling work is then calculated according to the relation:

$$\dot{W} = \frac{\dot{Q}}{\mathrm{COP}_c} = \frac{\dot{m}_2(h_2 - h_3)}{\mathrm{COP}_c} \tag{12}$$

where COP_c is the coefficient of performance of the system used to provide the sensible cooling necessary. A value of $\mathrm{COP}_c = 3$ has consistently been adopted in this study. In tandem with our least work definition in Section 2.2, $\dot{W}$ is normalized per unit outdoor air when calculating the second law efficiency.

3.2 Modeling results

By parametrically fixing the inlet and outlet states, the performance of the VCS is analyzed under different climate conditions. Figure 4 illustrates that the second law efficiency increases with increasing temperature and decreasing humidity. These results underscore the fact that this technology, while being more efficient at cooling, is highly inefficient at dehumidification as it necessitates the condensation of water, an energy-intensive process.

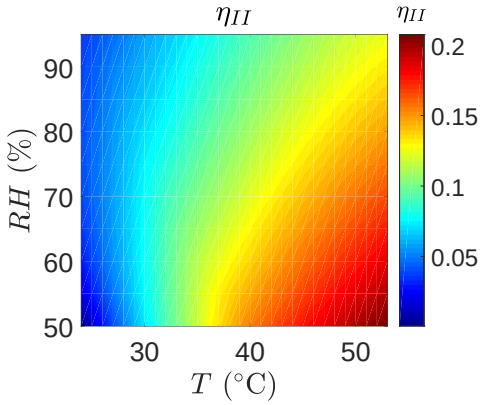

Figure 4: Performance of the VCS.

As our results indicate, this process is least efficient in low temperature and high humidity climates, and its performance improves as the conditions approach those of a hot and dry climate. In spite of its being most efficient under hot and dry conditions, the VCS system is challenged the most under such climates by alternative technologies as our assessment

of desiccant and membrane systems will demonstrate. The observation that this technology achieves a second law efficiency of around 20% at best suggests there is a significant opportunity for improvement.

4 Energy analysis for DCS

Compared to VCS, a desiccant-cooling system (DCS) avoids the limitation of having to lower the temperature to the dew point for dehumidification to occur. In addition, the ability of the DCS to dehumidify the air without the compressors needed in the VCS and MCS presents it with competitive advantages under some climate conditions as we explore next. This section addresses the development of thermodynamic models to describe desiccant-based technologies. Modeling is extended to investigate the effects of system integration and recuperation, and parametric studies are employed to uncover the prospects and limitations of this technology.

4.1 Thermodynamic model of desiccant-based dehumidification and cooling

Desiccant cooling is typically operated in two units, a desiccant dehumidifier and a cooling unit. The dehumidifier unit can be in the form of a washing tower with a liquid desiccant solution or in the form of a solid desiccant bed. Desiccant wheels, the focus of our analysis, are gaining popularity as a result of compact system sizes and controllable operation conditions for individual buildings or building zones. The cooling unit is operated using a traditional cooling coil, featuring chilled water for example, or an Indirect Evaporative Cooling (IEC) system as our discussion later shows.

4.1.1 Model development

As shown in Fig. 5a, the process air first undergoes dehumidification as it interacts with the desiccant layer, experiencing an increase in temperature due to the adsorption heat. A traditional cooling coil is employed to cool the hot dry air to the desired state. Desiccant dehumidifiers usually operate under high moisture removal rates; in order to fairly compare with other technologies, the humidity ratio at the outlet of the dehumidifier in this study is assumed to be the same as that required for other technologies to meet the design conditions given by state 3. The exhaust air stream denoted by state 4 is preheated with $\dot{Q}_{ad}$ to regenerate the desiccant.

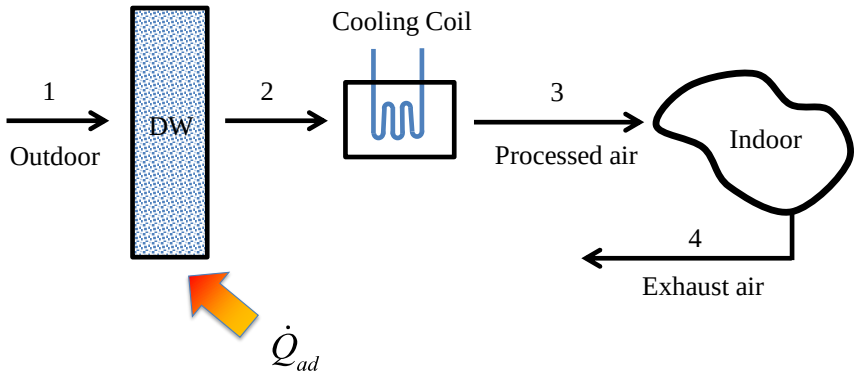

(a) Desiccant cooling process

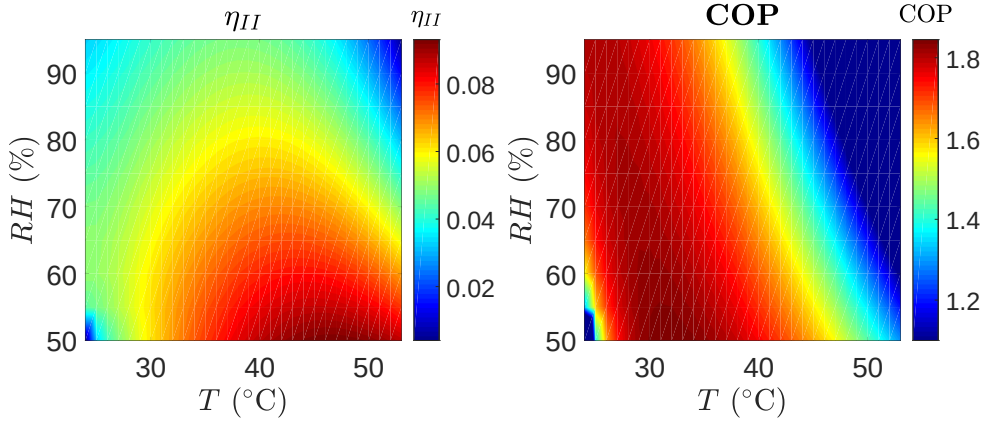

(b) Second-law efficiency and COP

Figure 5: Performance of the desiccant cooling process

Performing an energy analysis of the desiccant wheel requires adopting a numerical

model to predict the state of the streams leaving the wheel. Models in the literature largely fall into two categories: (1) coupled partial differential equation models accounting for the dynamic processes occurring within the wheel[44–46] and (2) simplified models based on correlations derived empirically.[47] More recently, Fu et al.[48] presented a micro-scale molecular dynamics sub-model coupled to a macro-scale heat and mass transfer sub-model. While the other models are more detailed and comprehensive, empirical models are sufficiently accurate for an energy analysis[33] and are adopted here. Based on the model adopted,[33,49] two empirical constants for effectiveness, η_{f1} and η_{f2}, are defined according to the correlations:

$$\eta_{f1} = \frac{f_{1so} - f_{1si}}{f_{1ei} - f_{1si}} \tag{13}$$

$$\eta_{f2} = \frac{f_{2so} - f_{2si}}{f_{2ei} - f_{2si}} \tag{14}$$

$$f_{1j} = -2865 T_j^{-1.49} + 4.344 \omega_j^{0.8624} \tag{15}$$

$$f_{2j} = T_j^{1.49}/6360 - 1.127 \omega_j^{0.07969} \tag{16}$$

Here, η_{f1} and η_{f2} are determined based on a desiccant wheel's specifications, s and e denote supply and exhaust states, i and o denote inlet and outlet states, and j refers to the stream index. Following the silica gel desiccant wheel configuration proposed by Zhang et al.[33,49] and summarized in the Appendix, the effectiveness constants are taken to be $\eta_{f1} = 0.30$ and $\eta_{f2} = 0.85$ herein. The modeling system is closed by solving for the unknown temperature in two states, the dehumidified and the regeneration air states.

According to the first law applied to the cooling system, the work input necessary to meet the cooling requirement is calculated as:

$$\dot{W}_{cool} = \frac{\dot{Q}}{\mathrm{COP}_c} = \frac{\dot{m}_3 (h_2 - h_3)}{\mathrm{COP}_c} \tag{17}$$

Another source of work input is the electric motor that provides rotational power for the

desiccant wheel. An experimental regression result[37] of the motor work $\dot{W}_m$ with rotational speed shows that the motor work accounts for less than 1% of the total work, which can reasonably be neglected.

Although desiccant cooling does not require any form of work input to separate the water vapor from the inlet air, desiccants can only adsorb finite amounts of water vapor before they reach a saturated state at which no more moisture can be harvested. A fraction of the surface area must be used to regenerate the saturated desiccant. Generally, the regeneration process requires heat input and a relatively high operational temperature, typically around 60 °C,[11,50] which cannot be accessed directly using ambient conditions absent solar thermal collectors or electrical heaters. The enthalpy difference between the inlet and outlet states to the heater is used to calculated the adsorption heat Q_{ad} in this model.[51,52] Assuming a heat pump is used to supply the regeneration heat with $\mathrm{COP}_h = 3$, the amount of regeneration work input $\dot{W}_{reg}$ is evaluated as:

$$\dot{W}_{reg} = \frac{\dot{Q}_{ad}}{\mathrm{COP}_h} \tag{18}$$

The total work input of the system is then the sum of regeneration work, cooling work and motor work.

4.1.2 Modeling results

The second-law efficiency and the COP of desiccant cooling are shown in Fig. 5b for varying outdoor conditions. The results demonstrate how both metrics decrease with rising humidity, with a minimum occurring under very hot and humid climates. These observations reflect the increase in latent cooling loads, raising the temperature and associated sensible cooling requirement of the processed air post-dehumidification. For a fixed relative humidity, however, our results indicate an initial boost followed by a decline in second-law efficiency, with this behavior becoming more prominent at higher humidities. These trends are a result of competition between cooling and necessary regeneration. Under lower outdoor temperatures, desiccant efficiency is lowered by the increase in cooling work imposed by the hot dry

air leaving the wheel, and large heat input necessary to reach the regeneration temperature. With rising temperatures, nonetheless, both cooling and regeneration work play a major role in lowering system performance under hot climates as observed.

Although desiccant cooling does not directly require any separation work, a large proportion of the work input is used for regeneration, and this results in much lower efficiency than the VCS. However, if the regeneration heat can be provided from heat recovery systems or solar power, the efficiency of the desiccant cooling could rise to nearly 40%.[11] When the outdoor air is very hot and humid, the outlet air temperature post-dehumidification will increase notably due to the adsorption heat. As a result, the system experiences two energy penalties as part of the dehumidification process: one for cooling the air considerably to reach the required supply conditions, and another for regenerating the desiccant. A stand-alone DCS will forgo the opportunity to recuperate the heat from the high temperature dehumidified air. The low efficiency calculated here reminds us of the importance of integrating a heat recovery system to improve efficiency and boost the technology's competitiveness.

4.2 DCS system integration

4.2.1 Design development

A stand-alone DCS cannot achieve optimal efficiency. To recuperate the heat from the hot dehumidified air, a heat exchanger is set up in an integrated design (shown in Fig. 6a) between the hot dehumidified air and the cool return air, saving energy for both cooling and regenerative heating.

In order to fulfill the requirement of humidity removal, we first need to determine whether the desiccant can adsorb the required amount of water vapor. This requirement has been validated using a detailed model of desiccant adsorption, presented in the Appendix. In this work, we assume the maximum capacity of the desiccant to absorb moisture is set by the desired humidity ratio removal rate, and thus $\omega_2 = \omega_3 = \omega_4$.

The effectiveness of the heat exchanger, ϵ_{HX}, defined in Eq. 19, determines how much

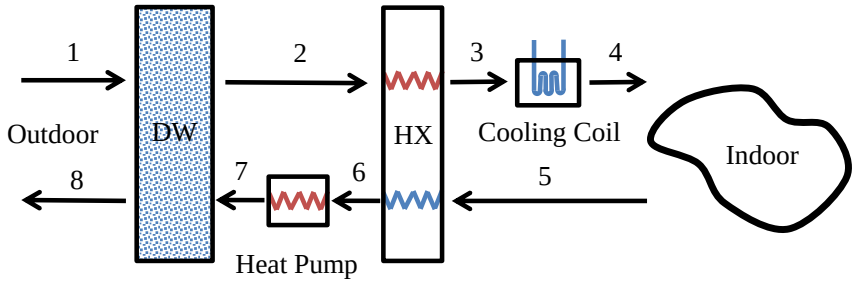

(a) Desiccant Cooling System

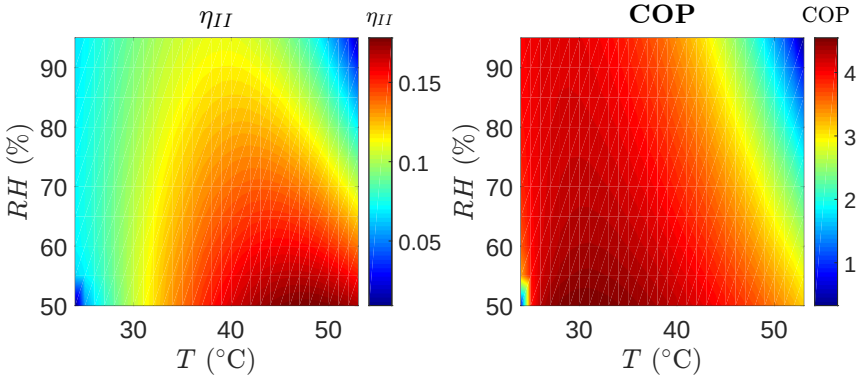

(b) Efficiency of the DCS with cooling coil system

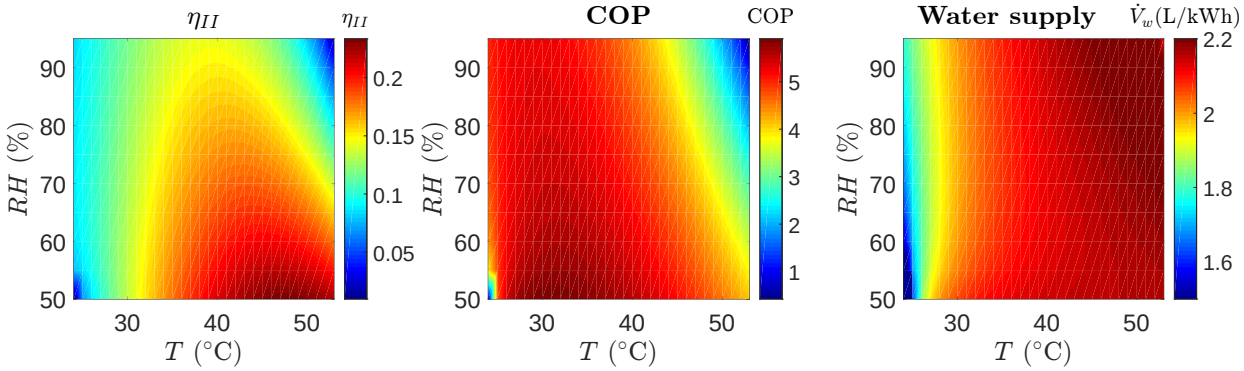

(c) Efficiency of the DCS with IEC system

Figure 6: Performance of the integrated DCS.

heat is recovered from the hot dehumidified air and how much additional cooling work is necessary to reach the desired supply conditions. Considering the limiting case of counter flow with a finite heat transfer rate and a finitely large exchange area, ϵ_{HX} is taken as 0.8.

$$\epsilon_{HX} = \frac{T_2 - T_3}{T_2 - T_5} \tag{19}$$

For the two streams across the heat exchanger, we can also arrive at the enthalpy equality

between inlet and outlet with the assumption of well-insulated walls for the heat exchanger, as Eq. 20 shows:

$$h_2 + h_5 = h_3 + h_6 \tag{20}$$

A cooling system, such as a conventional cooling coil or an IEC system, must be employed after the heat exchanger. As defined in Eq. 17, the cooling work provided by the cooling coil is calculated with the predefined COP_c. For the IEC system, the same approach is followed using its corresponding COP_{iec}, valued in a range of 10 to 25 according to previous research results.[53,54] Note that only sensible heat is removed by the IEC system.

In contrast to the dehumidification process, return air increases in humidity when flowing across the regeneration zone of the desiccant wheel. To guarantee the steady humidity removal of the water vapor from the outdoor air, the return air in the regeneration zone is assumed to drain out the adsorbed water vapor in the desiccant. The prerequisites to maintaining this performance are to make sure the temperature of the air in the regeneration zone exceeds the regeneration temperature, and to simultaneously ensure the exhaust stream is not saturated. Ensuring these conditions are met requires an additional heat source (e.g., heat pump or solar thermal collector) to further raise the temperature of the return air at state 6. The regeneration work is calculated with a heat pump COP_h of 3. Lastly, we assume that the pressure drop across the desiccant wheel is small and the corresponding pump work is negligible.

4.2.2 Modeling results

To investigate the effect of outdoor conditions on performance, we performed a parametric study by varying outdoor temperature and relative humidity. The rotational speed may be adjusted to guarantee that the humidity ratio of the dehumidified air matches indoor design conditions for different outdoor air conditions. Angrisani et al.[55] analyzed the effect of rotational speed on desiccant wheel performance, while Wang et al.[56] presented an optimal humidity control model (OHCM) to optimize desiccant wheel operation while satisfying

design constraints.

As shown in Fig. 6b and 6c, the integrated system experiences a boost in performance with the addition of a heat exchanger, while the performance trends remain similar to those of the component-level design. System performance drops with rising humidity due to the increase in both latent and sensible loads. While the heat exchanger raises system efficiency by enabling energy recuperation between the inlet and outlet streams, the rise in cooling work is still significant so that performance deteriorates with rising humidity. Furthermore, the presence of a heat exchanger is less significant at low temperatures and humidities as the temperature rise post-dehumidification becomes less severe. Given a heat exchanger's finite area and effectiveness, hot and humid climates place a similar limitation on the total energy the system can recuperate.

Substituting the conventional cooling coil with an IEC system raises the efficiencies by about 15%. However, improvement of the performance is not free as evaporative coolers will require a steady supply of liquid water to remove the sensible heat through evaporation. To put this in perspective, Fig. 6c shows the volume rate of water consumption in the unit of L/kW h work input. As the second-law efficiency becomes higher in hotter climates, the water consumption also rises. The requirement of large water supply limits the use of the IEC system to geographic locations where water is not scarce.

5 Energy analysis for MCS

Unlike vapor-compression or desiccant-based systems, the performance of membrane-based systems is governed by radically different operating principles. This section focuses on developing thermodynamic models for various membrane systems, starting with the simplest and then building up in complexity. Similar to our DCS analysis, system integration and recuperation are later incorporated to boost performance, and parametric studies are run to investigate the potential membranes offer given their isothermal operation.

5.1 Thermodynamic model of membrane-based dehumidification and cooling

Unlike other technologies, an outdoor air stream in the MCS is dehumidified by a hydrophilic semi-permeable membrane with a transmembrane vapor pressure difference. To simplify the analysis, the membranes in this study are assumed to be perfect membranes that allow only water vapor to permeate. This assumption presents a reasonable approximation as recent membranes developed by researchers have been reported to achieve a selectivity, or a water/air permeance ratio, of around 10,000.[20] Membranes with lower selectivity tend to require higher transmembrane pressures or larger areas to achieve the desired dehumidification effect. In addition, separation across the membrane is assumed to be isothermal and hydraulic losses are ignored for simplicity.

5.1.1 Model development

To demonstrate the concepts underlying the MCS, we start with the simplest configuration depicted in Fig. 7a. Hot and humid air enters the membrane module with predefined conditions and the membrane acts to dehumidify the process air isothermally, such that the humidity ratio at the module outlet matches design targets. Thereafter, a traditional cooling coil, as encountered in the DCS, is employed to sensibly cool the dry air to the desired temperature, completing the dehumidification and cooling process. A vacuum pump is applied on the sweep side to drive mass transport. Similar to gas separation, the flux of water across the membrane is primarily governed by the transmembrane vapor pressure difference. The membrane designs proposed in this work and others take advantage of this principle to minimize the transmembrane pressure, which directly affects pumping work, while keeping the transmembrane vapor pressure at a maximum.

Similar to the setup proposed by Bui et al.,[20] P_6 is taken to equal atmospheric conditions, while P_5 is set at 1 mbar. Better membranes might be able to reduce the necessary work with higher permeances. Two major constraints on the vapor pressure should always be satisfied

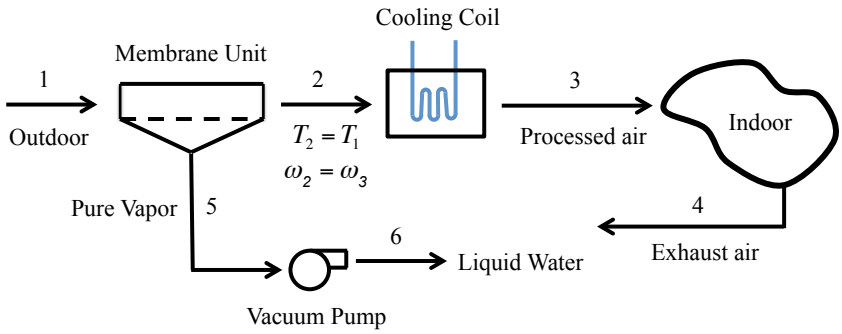

(a) MCS design with a vacuum pump

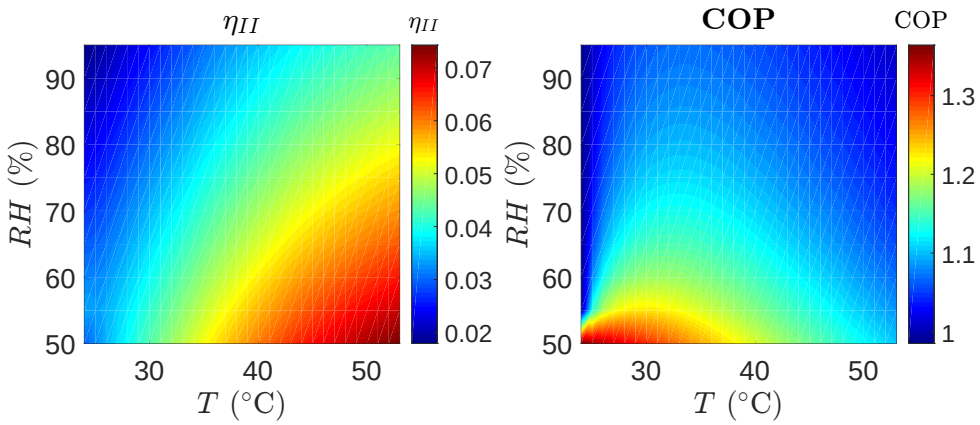

(b) Second-law efficiency and COP of the MCS with a vacuum pump

Figure 7: Performance of the MCS with a vacuum pump.

during membrane operation in dehumidification. First, the pressure at all points should not exceed the saturation pressure, P_{sat}, at the ambient temperature to avoid condensation. Second, the vapor pressure on the sweep side should always be lower than the feed side to drive transport.

Throughout this paper, the isentropic efficiency of the vacuum pump is assumed to be 0.9. The design in Fig. 7a suffers from undesirable condensation in the pump. Given its low volumetric density, vapor compression is also associated with higher energy penalties. As an alternative, we propose a two-stage pumping approach inspired by the Rankine cycle and first introduced by Cladridge and Culp,[57,58] where the vapor will be condensed before complete compression.

As Fig. 8a illustrates, pure vapor is first compressed from state 5 to 6 before it is condensed and pumped back to ambient conditions. In this design, the first pumping stage

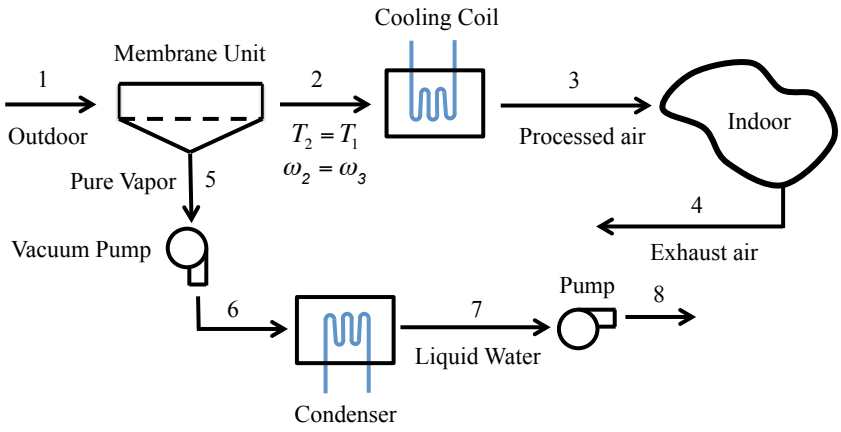

(a) MCS design with a condenser pump

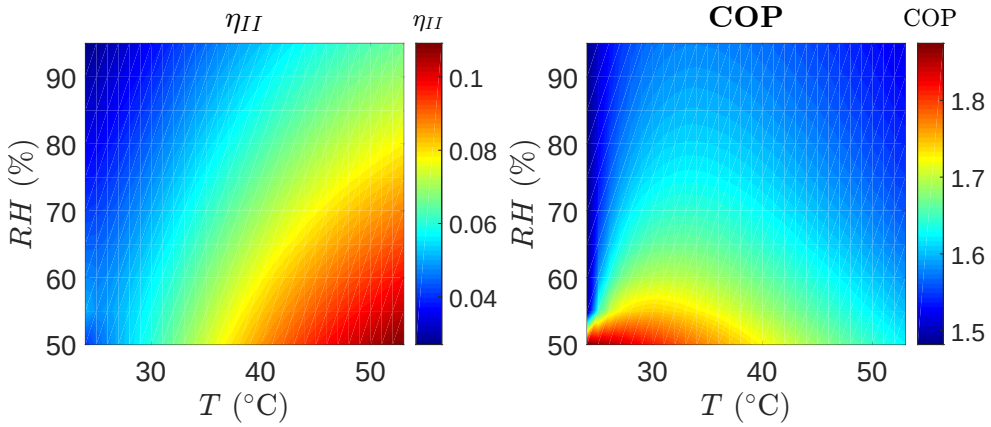

(b) Second-law efficiency and COP of the MCS with a condenser pump

Figure 8: Performance of the MCS with a condenser pump.

serves to avoid potential freezing of the vapor in the condenser as can be ascertained from a phase diagram. The values of P_5 and P_6 were set at 1 and 20 mbar herein. Although the work of the second-stage pump is expected to be small, the energy cost of condensation, as calculated by Eq. 21, is still high.

$$\dot{Q}_{con} = \dot{m}_w(h_6 - h_7) \tag{21}$$

5.1.2 Modeling results

Figure 7b shows the results generated for the MCS configuration with a vacuum pump, which show that the second law efficiency increases with increasing temperature and decreasing

humidity. Given the high compression ratio of the proposed configuration, the compression work is a significant portion of the energy requirement, often displaces any advantages of using the MCS over the VCS, and makes this configuration unpractical in an HVAC context. For most environmental conditions studied, the COP of this MCS design did not outperform that of the VCS.

Implementing a two-stage pumping design with a condenser boosts performance considerably as Fig. 8b attests, underscoring the importance of reducing the compressor work to make membranes more competitive. While in both technologies harvested vapor is condensed, the proposed MCS is at an advantage relative to the VCS by not requiring the process air to be unnecessarily cooled to the dew point temperature to achieve the dehumidification desired.

Similar to the VCS, system performance, as measured by the second law efficiency in Fig. 8b, improves with increasing temperature and decreasing humidity since our analysis accounts for the cost of condensation. These trends look different when this energy penalty is neglected by assuming that the ambient environment acts as a heat sink, with the MCS performance remaining high at higher humidities and second law efficiencies falling in the range of 12%–28%. Such an analysis, however, would be limited to relatively cooler climate zones, and is not generalizable. Any potential increase in capital cost associated with the additional heat exchangers necessary should also be considered.

In summary, modeling results indicate that high compression ratios are not only impractical in an HVAC context but also undermine the overall system performance. Any economically-feasible implementation of membrane technology in dehumidification and cooling must address this problem a priori. A more subtle conclusion is that membranes are more likely to become competitive through more advanced system design and integration specifically aimed at exploiting their characteristics more effectively, as we explore next.

5.2 MCS system integration

5.2.1 Design development

While our analysis shows that a stand-alone MCS has lower efficiency than VCS, a membrane system differs from vapor-compression in many respects. One advantage the MCS possesses over the VCS and the DCS is its ability to separate water vapor at high purity. This opens up the opportunity for water reuse in evaporative cooling, direct or indirect, whose operation can be sustained solely by the harvested water. Water recovery in this form can act as a form of energy recuperation by which a portion of the energy spent achieving separation is recovered through evaporative cooling. On the other hand, water recovered in the VCS cannot be reused in evaporative cooling since the air stream is already highly humid during pre-processing, and relatively cold during post-processing.

Employing direct evaporative cooling would require air to be dried beyond the design conditions for it to produce supply air at specified conditions. Accordingly, a design with a direct evaporative cooler is likely to suffer from two opposing trends. Such a design will reduce the energy penalty of sensible cooling, while adding to the energy penalty of membrane separation and sweep condensation. Since an evaporative cooler can only cool an air stream along a constant enthalpy line, a cooling coil might still be required to meet design conditions.

Figure 9a depicts a design similar to the one discussed, employing a cooling system with an evaporative cooler (direct or indirect) and an additional heat exchanger to increase energy recovery and raise efficiency. This design has been modeled following the framework and assumptions developed throughout this work. Another alternative to investigate will be replacing the IEC system with both a direct evaporative cooling system and a cooling coil to satisfy the cooling requirements.

Instead of employing membranes to mechanically separate the vapor prior to condensation, Fig. 10a presents an alternative approach combining a membrane total heat recovery

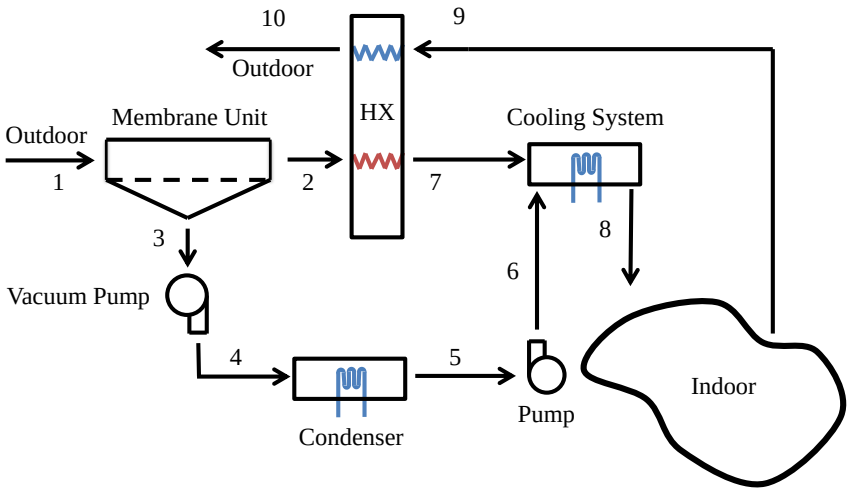

(a) Membrane-evaporative cooler hybrid

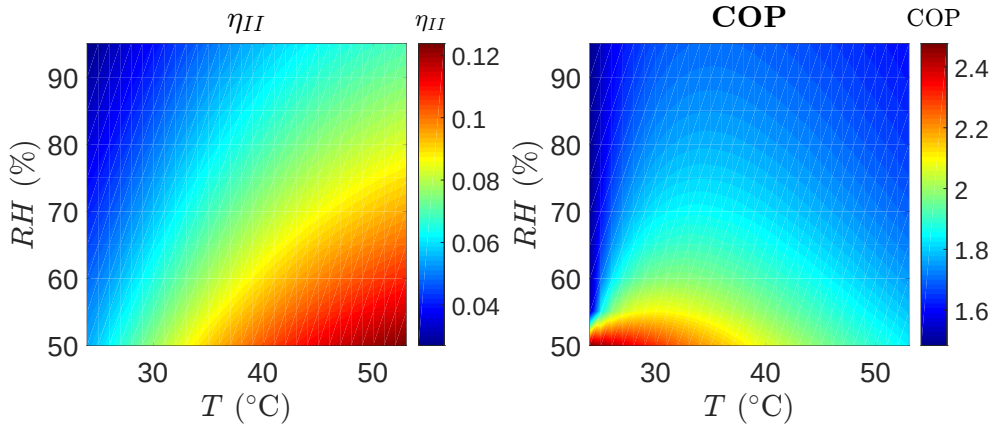

(b) Second-law efficiency and COP of the membrane-evaporative cooler hybrid

Figure 9: Performance of the Membrane-Evaporative Cooler Hybrid

with the DCS analyzed previously in Section 4.2. Unlike the previous design, this MX-DCS hybrid, reviewed by Zhang,[16] is thermally driven and allows the incoming and outgoing streams to exchange heat and moisture through a membrane exchanger. The result is greater energy recuperation and lower sensible and latent loads imposed on the DCS regardless of climate as our results will demonstrate later. The performance of the membrane exchanger is dictated by two empirical constants, the sensible effectiveness and latent effectiveness, defined by Eqs. 22-23 following the notation in Fig. 10a. Following studies reported in the literature[33] based on current state-of-the-art, a sensible effectiveness $\epsilon_S = 0.8$ and a latent effectiveness $\epsilon_L = 0.9$ were adopted herein. The DCS subsystem is modeled as explained

previously.

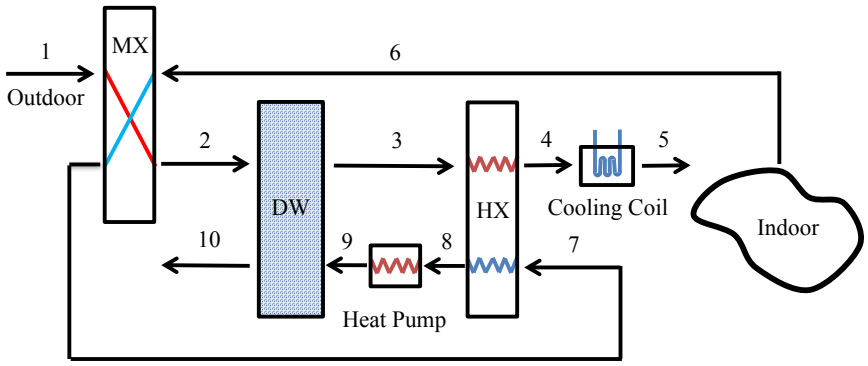

(a) MX-DCS total heat recovery hybrid

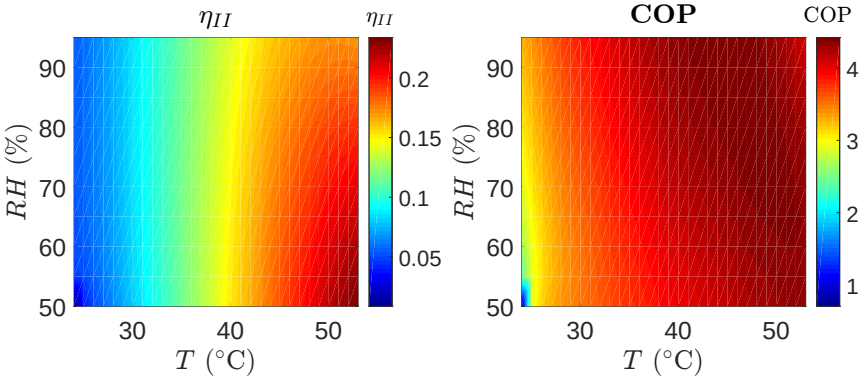

(b) Efficiency of the MX-DCS total heat recovery hybrid with cooling coil system

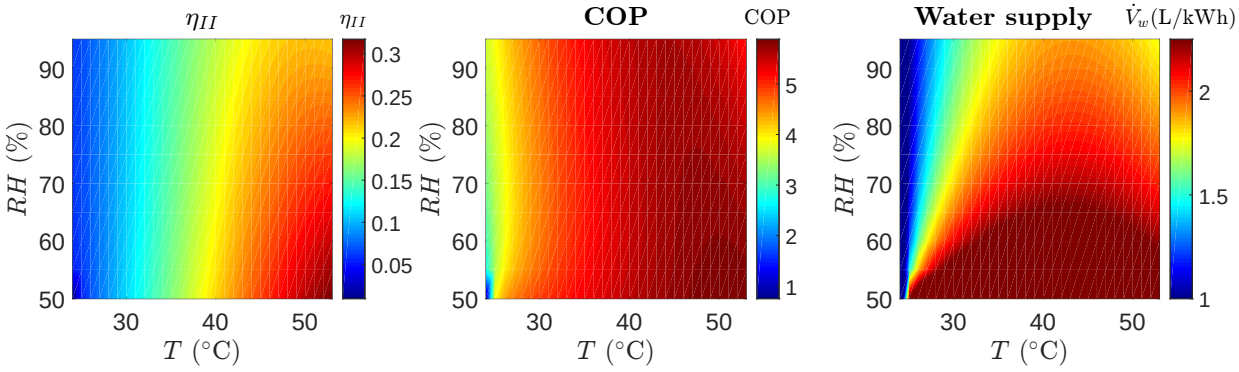

(c) Efficiency of the MX-DCS total heat recovery hybrid with IEC system

Figure 10: Performance of the MX-DCS total heat recovery hybrid.

$$\epsilon_S = \frac{T_1 - T_2}{T_1 - T_6} \tag{22}$$

$$\epsilon_L = \frac{\omega_1 - \omega_2}{\omega_1 - \omega_6} \tag{23}$$

Figure 11a illustrates our last proposed design, inspired by another invented by Claridge and Culp[59] and reviewed by Woods,[15] that also aims to achieve cooling and dehumidification absent any condensation. The system features two membrane modules, one that extracts humidity and one that actively rejects it back to the outdoor air. For vapor harvested in the top module to leave through the bottom module, the vapor pressure on the sweep side (P_9) should exceed that of the rejected air ($P_{7,v}$) while still being below saturation pressure (P_{sat}), following Eq. 24.

$$P_{7,v} < P_9 < P_{sat} \tag{24}$$

To ensure flux continuity (no vapor build-up) in the system, the vapor pressure difference across both membranes modules should be set equal, leading to the relationship:

$$P_8 + P_9 = P_{1,v} + P_{6^*,v} \tag{25}$$

To fully close the system of equations, the pressure at state 8 is defined according to a preset compression ratio referred to as r_p, defined in Eq. 26 and given a value of 5 herein. A larger compression ratio decreases the pressure on the sweep side of the top module, increasing the flux, but only at the expense of increased energy penalty.

$$r_p = \frac{P_9}{P_8} \tag{26}$$

One important aspect of this design is the on-demand heat pump, which reduces the risk of membrane fouling by ensuring no condensation occurs in the lower module. The heat pump is only operated when the amount of vapor harvested from the outdoor air exceeds the additional amount allowable at state 6 before saturation. When this condition is met, the temperature is then raised to state 6*, such that the air stream exits the lower module at state 7 as a saturated air/vapor mixture. This situation is likely to occur when operating

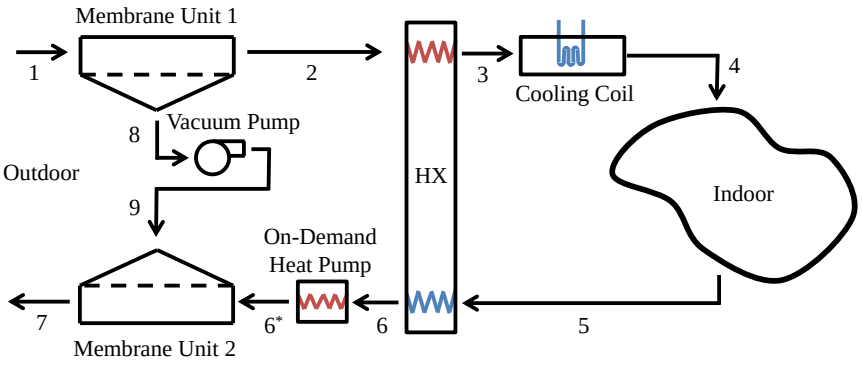

(a) Integrated membrane-recuperation system

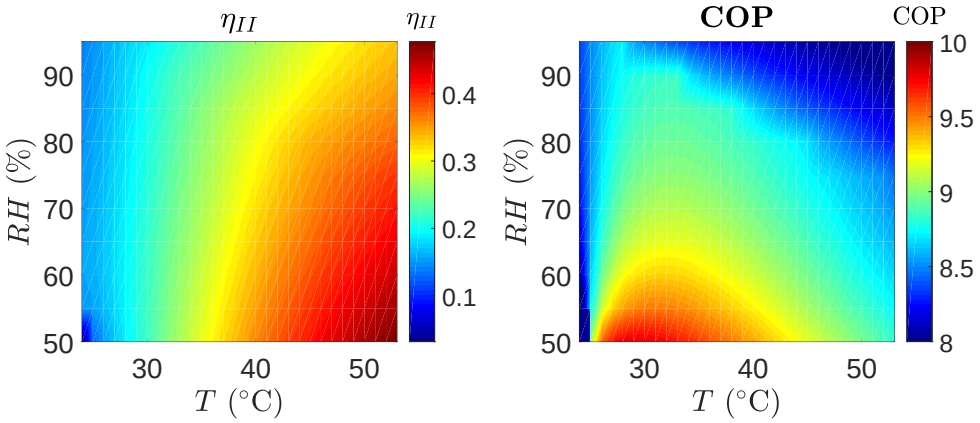

(b) Second-law efficiency and COP of the integrated membrane-recuperation system

Figure 11: Performance of the integrated membrane-recuperation system.

at high humidity, such that cooling the air stream could induce condensation. The rest of the system operates as explained previously.

5.2.2 Modeling results

Similar to the VCS and the DCS, parametric studies were run to investigate the prospects and limitations of the proposed MCS designs. For the design proposed in Fig. 9a featuring a direct evaporative cooler, it remains unclear what fraction α of ω_1 should be harvested to achieve optimal performance. Running sensitivity analyses reveals that η_{II} decreases monotonically with increasing α, starting from the minimum α necessary to meet design conditions. For this reason, α was assigned its minimum value herein. These results indicate

that employing a direct evaporative cooler is not justified as the penalty incurred from the additional dehumidification and condensation necessary outweighs any potential savings (unless the cost of condensation could be dropped as discussed previously).

Apart from this observation, the MCS remains at an advantage relative to other technologies as the harvested water could be employed in indirect evaporative cooling. Modeling results indicate that the amount of water harvested at the minimum α was always sufficient to meet the desired cooling loads using an IEC system. Further simulation results reveal that system performance is not a strong function of the heat exchanger, which could be discarded in this case to minimize CAPEX. This observation is in contrast to the DCS, whose performance is strongly affected by the presence of an efficient heat exchanger to recover the adsorption energy for use in desiccant regeneration, and makes the MCS more attractive than the DCS from a CAPEX standpoint.

Figure 9b depicts the system's performance in response to varying climate conditions. Comparing these results to those reported previously for the corresponding component design in Fig. 8b reveals that only a minor improvement was attained through better system integration, which focused on lowering the processed stream's sensible loads by incorporating a heat exchanger and an IEC system. Rather than the sensible loads, these results suggest that vapor condensation dominates the energy consumption. This result, which is further confirmed by assuming free condensation to realize an approximately twofold performance improvement, is attributed to the membrane's isothermal operation.

Unlike the DCS, the sensible cooling loads post-dehumidification in MCS are minimal, particularly under moderate climates. For this reason, the second law efficiency does not drop at higher temperatures (as encountered in DCS), implying that MCS is not bound by the same set of constraints as DCS: a finite heat exchanger effectiveness and considerable sensible loads. Under the assumption that the condensation energy will contribute to the energy cost of running the system, it appears that a primary way for membrane systems to become more competitive is to rid themselves of condensation. Unlike the VCS and the

DCS, membranes are the only technology that offers this capability, as demonstrated by our next designs.

Given its ability to recuperate latent loads, the performance of the MX-DCS hybrid, shown in Fig. 10b, indicates only a slight decrease in efficiency and COP with higher humidities. Unlike the DCS system, the improved recuperation also allows the efficiency and COP to increase monotonically for the MX-DCS hybrid with rising temperatures. While the membrane exchanger operates passively in this design, the absence of a compressor lowers the driving force across the exchanger and could place limitations on its performance under a finite membrane area.

Modeling results for the integrated membrane-recuperation system are reported in Fig. 11b, showing significant improvement relative to the other systems investigated. This notable improvement is another manifestation of the limitations condensation imposes and the effect of latent loads on overall performance. For most conditions studied, system performance improves with increasing temperature, and is not a strong function of outdoor humidity. Increased humidity does not directly contribute to energy consumption as the limitations of a finite membrane area were neglected in the study. These trends break down discontinuously at higher humidities once the on-demand heat pump is operated as shown by the discontinuous lines for efficiency in Fig. 11b.

Another advantage of this design is that it implements energy recuperation in two forms. First, a heat exchanger recovers energy in the form of sensible heat. Second, the exhaust air stream is intentionally passed through the bottom module (rather than running the bottom module on outside air) since it is expected to have a lower humidity ratio. A lower humidity ratio increases the flux across the bottom module, allowing the same amount of water vapor to be rejected at lower energy costs. More importantly, however, the performance of this MCS system, while it appears favorable, was found to be very sensitive to the compression ratio employed, underscoring the need for research on developing selective membranes to achieve the necessary dehumidification given a finite membrane area under lower compression ratios.

6 Comparisons and discussion

The previous sections focused on specific technologies. We now adopt a more holistic approach, collectively considering the systems proposed while investigating how the different technologies fare with respect to one another. The psychrometric chart is used as a vehicle for qualitative assessment of the different technologies and a more quantitative analysis follows. The section concludes with a case study investigating the potential of next-generation HVAC systems in different cities worldwide relative to the VCS, showing that the optimal design would ultimately be a function of climate conditions and resource availability.

6.1 Component-level comparison

As shown in Fig. 12, states 1 and 6 refer to the initial outdoor and supply air conditions. Different technologies follow different paths (depicted by arrows) from state 1 to 6. The fact that these states represent actual thermodynamic states implies that the net enthalpy change (per unit dry air of the processed air) remains equal across all technologies as the air is processed from state 1 to 6. More complicated paths associated with greater enthalpy changes, nonetheless, introduce larger energy transfers and pose an increased potential for inefficiencies. This becomes even more evident from our results, showing the energy penalty associated with technologies employing such paths to be greater.

The VCS follows the path 1–2–3–6, consuming considerable energy to cool the air, reach the dew point temperature, and sustain condensation. The processed stream is later conditioned again to reach the desired state. It is this over-cooling to the dew point that makes the VCS suffer from a relatively lower efficiency. The DCS follows the path 1–4–6, employing no work input for air-vapor separation, while still needing to cool the hot dehumidified air from a relatively higher temperature level. Not apparent from the psychrometric chart is the additional work necessary for regeneration, however. The MCS follows the shorter path 1–5–6, invoking the highly efficient isothermal separation process, albeit suffering from

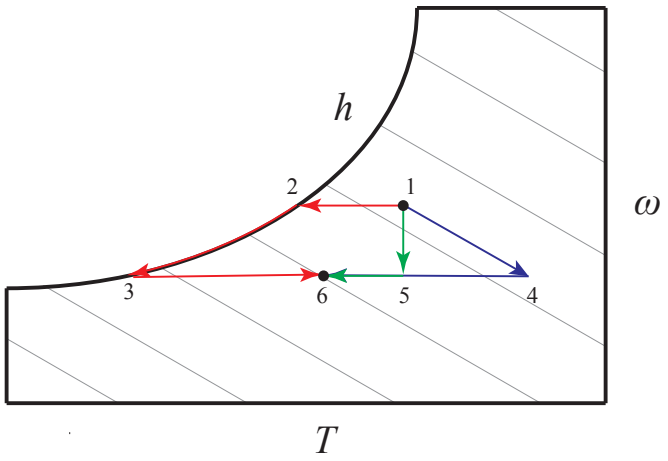

Figure 12: Psychrometric chart of dehumidification and cooling processes. Arrows in red refer to the VCS, blue to the stand-alone DCS, and green to the stand-alone MCS.

considerable compressor work to support this process. As with the DCS, the psychrometric chart does not reveal whether the harvested vapor is condensed.

A quantitative comparison of the different technologies in Fig. 13 shows that the stand-alone DCS is more efficient than MCS at low temperatures, whereas MCS tends to be more efficient at high temperatures and more evidently with rising humidities. While DCS suffers from the energy penalty associated with adsorption heat, this penalty is outweighed by the cost of condensation in MCS at low temperatures, making the DCS more efficient. With rising humidity and temperature, however, the trend is reversed as adsorption heat and the additional regeneration work necessary limit DCS performance relative to MCS. Interestingly, comparing both stand-alone technologies to the conventional VCS in Fig. 13 reveals that both fail to outperform the VCS under most climate conditions, with a few exceptions in cooler and drier climates. These results remind us again of the significance of system design and integration in making next-generation HVAC technologies more competitive.

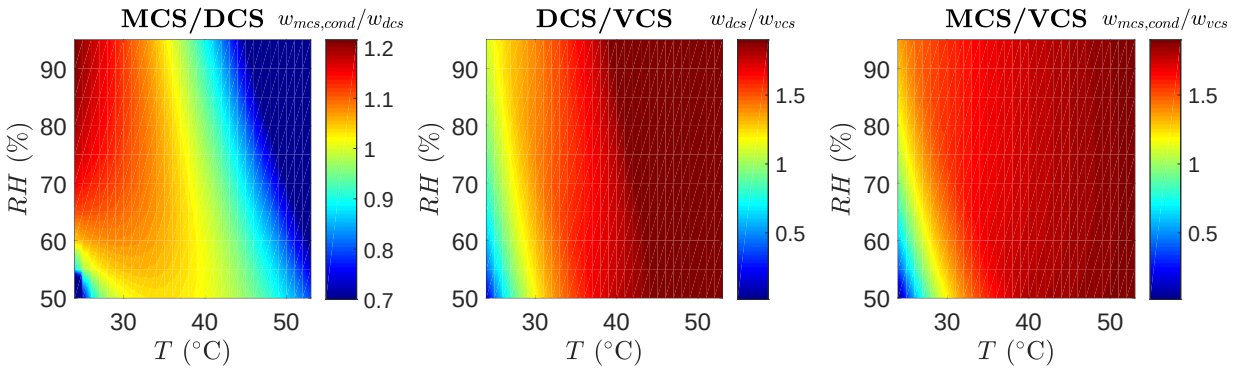

Figure 13: Comparisons of the work input among different stand-alone technologies.

6.2 System-level comparison

With the greater design flexibility offered by system integration and energy recuperation, quantitatively comparing the energy costs associated with each design, as shown in Fig. 14, becomes necessary to ascertain the optimal design for a given set of climate conditions. Of the proposed designs with the three technologies studied, the VCS consumes the most work (nearly 5–10 times that of the theoretical minimum work) due to its coupling of sensible and latent heat removal.

Both DCS designs achieve significant energy savings compared to stand-alone units. The regeneration work input is largely reduced with the heat recovery from the hot dehumidified air. DCS with a cooling coil or IEC system consistently outperformed VCS by decoupling the sensible and latent loads under most climate conditions. With more extreme climates, the increasing adsorption heat and its associated rise in sensible cooling, however, makes VCS more favorable. The DCS with IEC outperforms the other DCS design featuring a conventional cooling coil, although a steady intake of cool liquid water could pose a challenge in locations experiencing water scarcity. Coupling a membrane total heat recovery to the DCS with IEC provided a further design improvement, producing even greater recuperation and efficiencies approaching 30% as shown in Fig. 10c.

Likewise, all MCS designs improve energy efficiency with respect to the initial stand-alone units, and bring their own advantages in practical use. As apparent from our analysis,

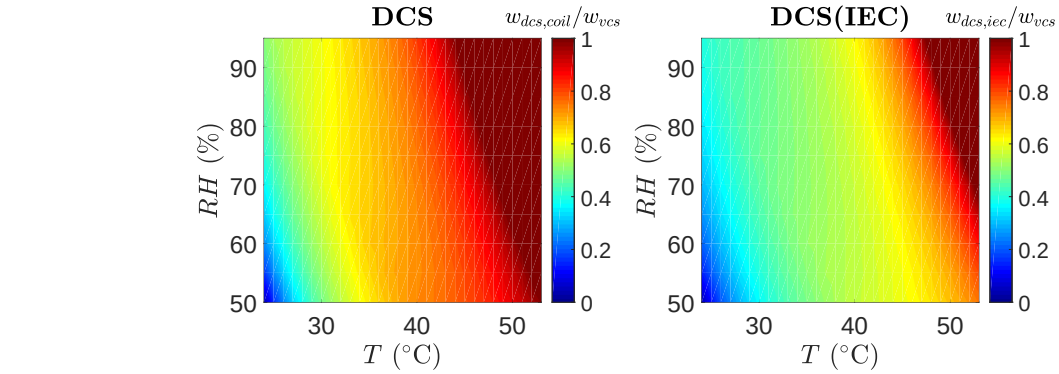

(a) Comparisons of the DCS systems to the VCS

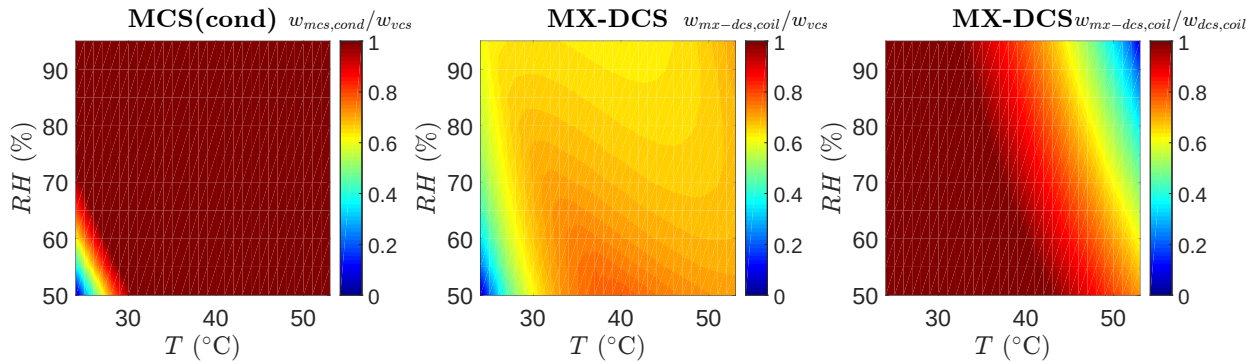

(b) Comparisons of the MCS systems to the VCS

Figure 14: Comparisons of the work input among different system designs.

the integrated MCS with a condenser pump (Fig. 9a) can boost its efficiency by recuperating separated water for use in the IEC system, which will be preferable in regions with water shortage. The integrated membrane-recuperation system (Fig. 11a) stands out for its notable cost-effectiveness under lower compression ratios. In order to achieve a stable performance, the selectivity of the membrane to water needs to be relatively high, such that operation under low compression ratios is feasible (assuming a finite membrane area) and back-flow from the exhaust air does not occur. Of all proposed designs, the first MCS design is evidently the least efficient due to vapor condensation as shown in Fig. 14b. Achieving free condensation as discussed previously could potentially improve this technology's prospects and make it more competitive.

As our results indicate, employing a membrane total heat recovery with DCS can mitigate this pitfall, making VCS less favorable, while boosting performance under such climate

conditions. The more uniform profile for the MX-DCS hybrid in Fig. 14b is attributed to the membrane exchanger, which mitigates much of the variance in cooling loads that would alternatively result from the varying climate conditions. This result underscores the potential of membrane total heat recovery to boost HVAC performance, while allowing for a more robust performance with varying climates.

The slight drop in performance experienced under moderate climates sheds light on the competition between the membrane exchanger and heat exchanger in the MX-DCS hybrid. While the membrane exchanger alleviates the cooling loads handled by the DCS, the rising temperature of the exhaust stream given by State 7 limits the performance of the heat exchanger. Under moderate climates, the benefit from decreasing the cooling loads using a membrane exchanger is outweighed by lost potential of heat recovery following the DW, causing an increase in the cooling and regeneration work necessary to run the system.

6.3 Case study

As can be observed from the parametric studies presented, the work input and energy efficiency of the different technologies and designs vary considerably with outdoor conditions. We end this section with a case study assessing the performance of the presented technologies. Table 1 lists four cities in different climates, characterized by outdoor temperature and relative humidity averaged over summer days, and summarizes system performance as a guide to choosing energy-efficient and practical technologies for a given climate.

Table 1: Performance of different system designs in different geographical locations.

City	T (°C)	RH (%)	$w_{dcs}(w_{dcs,iec})/w_{vcs}$	$w_{mcs,cond}/w_{vcs}$	$w_{mx-dcs}(w_{mx-dcs,iec})/w_{vcs}$
Dubai	45	55	0.800 (0.609)	1.59	0.718 (0.527)
Las Vegas	40	40	0.701 (0.535)	1.32	0.808 (0.543)
New York	24	65	0.320 (0.259)	0.798	0.426 (0.383)
Singapore	31	85	0.617 (0.477)	1.47	0.665 (0.534)

For all cities considered, the VCS was outperformed by the alternatives presented, except

for the MCS with condenser design, which only outperforms VCS under moderate climates. The reader should note, however, the optimal choice of technologies and designs for dehumidification and cooling will ultimately depend on both the local climate and availability of resources (both water and energy).

In Dubai (tropical desert climate), for example, DCS saves 20% of the energy consumption, whereas MX-DCS saves 30% relative to VCS. Introducing an IEC system in place of the cooling coil significantly boosts system performance with the MX-DCS reducing the energy consumption to about half of the VCS system. Of all cities considered, Dubai featured the hottest average temperature, which combined with the absorption heat, placed greater pressure on the cooling system employed. For this reason, the payoff from employing an IEC was largest in Dubai when ignoring the cost of water consumed. The scarcity of freshwater in Dubai places serious economic constraints on IEC adoption. Future developments in HVAC design focused on renewable energy, such as solar-powered regeneration, could bring about even more energy savings, catalyzing technology adoption in similar climates.

For Las Vegas (subtropical arid climate), where humidity is relatively lower, DCS proves to be the most efficient option as the MX-DCS performance deteriorates when the competition between the membrane exchanger and heat exchanger encountered previously in Section 6.2 becomes more prominent. Incorporating an IEC system in place of the cooling coil also lowers the energy consumption by 50% relative to VCS. Taking CAPEX considerations into account might justify adopting DCS over MX-DCS under similar climates.

In New York (subtropical humid climate), all designs considered outperformed VCS. Of these three designs, DCS stands out with about 70% reduction in overall energy consumption relative to VCS. Employing IEC could potentially boost performance even further. MX-DCS is challenged again under these climate conditions, underperforming DCS.

Singapore (tropical oceanic climate), on the other hand, features a similar performance for both DCS and MX-DCS (with both outperforming VCS), although CAPEX considerations potentially make DCS more attractive. While employing IEC is expected to benefit

system performance, the scarcity of water resources in Singapore places considerable limitations on IEC adoption. Similar to Dubai, future developments in solar-powered designs are expected to further technology adoption in this part of the world.

7 Conclusions

A framework based on fundamental thermodynamic principles was developed to enable systematic comparisons of three dehumidification and cooling technologies: the conventional VCS, the DCS, and the MCS. This work has extended our understanding of current and next-generation HVAC technologies, assessed their merits and limitations based on a common framework, and uncovered the situations in which a given design might outperform others. While previous work has primarily been focused on one technology, our work was aimed at offering a parallel treatment of current and next-generation technologies under varying climates to help guide technology selection.

The key findings of this work include:

1. The least work of dehumidification and cooling increased with temperature and more notably with humidity as the sensible and latent loads increased. The least work considering a condensed waste stream always exceeded that considering a saturated air/vapor waste stream. The difference, which became less significant with rising outdoor humidity, was consistently below 25%.

2. The second-law efficiency of the VCS increased with rising temperature and falling humidity, indicating its inefficient dehumidification performance (relative to cooling). While VCS performed best under hot and dry climates, our results indicate this is also where it is challenged the most by competitors. The second-law efficiency, which did not exceed 20%, suggests a great potential for improvement in the field.

3. Despite the inherent inefficiency of VCS, current DCS and MCS technologies can only

compete with VCS when proper system integration and energy recuperation are implemented.

4. At the component level, the second-law efficiency and COP of the DCS decreased with rising temperatures and humidities as the latent loads before and sensible loads after dehumidification continued to increase. Under fixed humidity, a tradeoff between the regeneration work and cooling work was observed, with the latter playing a more prominent role at higher temperatures. The lack of an energy recuperation mechanism imposed two penalties on the system: (1) desiccant regeneration and (2) significant cooling loads post-dehumidification.

5. While performance trends did not change considerably, integrating a heat exchanger boosted DCS performance, particularly at hotter/more humid climates. The increase in cooling loads post-dehumidification attributed to the adsorption heat was still notable, however, causing performance to deteriorate with humidity. Employing an IEC system raised efficiency by 15% at the expense of freshwater consumption.

6. For the MCS stand-alone design with vacuum pump, the high compression ratios associated with the design were found to be impractical. Instead, employing a two-stage pumping design with condenser notably improved performance. Neglecting the cost of condensation dramatically boosted performance, but the assumption's validity was not generalizable across all climates.

7. For the integrated MCS design with condenser, performance improved as condensed water was employed in cooling. Harvesting vapor in excess of the HVAC design requirement for use in direct evaporative cooling was counterproductive, making IEC with minimal vapor harvesting the best option. The small improvement noted indicated vapor condensation dominates energy consumption in this design. Of all integrated designs proposed, this design was the least efficient.

8. Avoiding condensation through an integrated-membrane design boosted performance considerably by employing two forms of recuperation. Ignoring the limitations of finite area made performance appear less sensitive to humidity. This trend changed at higher humidities, however, as operating a heater became necessary to avoid condensation.

9. Technologies with more complicated paths on the psychrometric chart were associated with greater enthalpy changes and energy transfers, leaving a greater potential for inefficiencies to jeopardize performance.

10. At low temperatures, stand-alone DCS outperformed stand-alone MCS, which suffered from the high cost of condensation. Higher temperatures and humidities placed greater limitations in the form of sensible cooling and regeneration energy on the stand-alone DCS, however, making stand-alone MCS more favorable.

11. Combining membrane total heat recovery with DCS raised efficiencies up to 30%. The membrane exchanger reduced cooling load variation and led to a more robust performance. The hybrid was less effective under moderate climates as a result of the competition between the heat and membrane exchangers. Limits on finite membrane area could pose further challenges to this design.

12. For all cities considered in the case study, VCS was consistently outperformed by competitors to varying extents. The optimal choice of technologies and designs was shown to be dictated by climate and natural resources.

Acknowledgement

This research is supported by the National Research Foundation (NRF) – Singapore under its Campus for Research Excellence and Technological Enterprise (CREATE) programme. The Center for Environmental Sensing and Modeling (CENSAM) is an interdisciplinary research

group (IRG) of the Singapore MIT Alliance for Research and Technology (SMART). The authors also acknowledge Dr. Jaichander Swaminathan for helpful discussion.

References

(1) Ghoniem, A. F. Needs, resources and climate change: Clean and efficient conversion technologies. *Progress in Energy and Combustion Science* **2011**, *37*, 15–51.

(2) Griffin, J. P. Montreal protocol on substances that deplete the ozone layer. International Lawyer (ABA). 1988; p 1261.

(3) Solomon, S.; Qin, D.; Manning, M.; Chen, Z.; Marquis, M.; Averyt, K.; Tignor, M.; Miller, H. *Contribution of working group I to the fourth assessment report of the intergovernmental panel on climate change 2007*; Cambridge University Press, Cambridge, 2007.

(4) UNEP, Proposed amendment to the montreal protocol submitted by Canada, Mexico and the United States of America. 2013.

(5) Commission, E. European commissioner connie hedegaard welcomes major step forward to reduce some of the most dangerous greenhouse gases. 2013.

(6) Chua, K.; Chou, S.; Yang, W.; Yan, J. Achieving better energy-efficient air conditioning - A review of technologies and strategies. *Applied Energy* **2013**, *104*, 87 – 104.

(7) Goetzler, W.; Zogg, R.; Young, J.; Johnson, C. Energy savings potential and RD&D opportunities for non-vapor-compression HVAC technologies. 2014.

(8) Goetzler, W.; Zogg, R.; Young, J.; Johnson, C. Alternatives to vapor-compression HVAC technology. *ASHRAE Journal* **2014**, *56*, 12.

(9) Misha, S.; Mat, S.; Ruslan, M.; Sopian, K. Review of solid/liquid desiccant in the drying applications and its regeneration methods. *Renewable and Sustainable Energy Reviews* **2012**, *16*, 4686 – 4707.

(10) Daou, K.; Wang, R.; Xia, Z. Desiccant cooling air conditioning: A review. *Renewable and Sustainable Energy Reviews* **2006**, *10*, 55–77.

(11) La, D.; Dai, Y.; Li, Y.; Wang, R.; Ge, T. Technical development of rotary desiccant dehumidification and air conditioning: A review. *Renewable and Sustainable Energy Reviews* **2010**, *14*, 130–147.

(12) Angrisani, G.; Capozzoli, A.; Minichiello, F.; Roselli, C.; Sasso, M. Desiccant wheel regenerated by thermal energy from a microcogenerator: Experimental assessment of the performances. *Applied Energy* **2011**, *88*, 1354 – 1365.

(13) Angrisani, G.; Minichiello, F.; Roselli, C.; Sasso, M. Experimental analysis on the dehumidification and thermal performance of a desiccant wheel. *Applied Energy* **2012**, *92*, 563 – 572.

(14) Niu, J.; Zhang, L.; Zuo, H. Energy savings potential of chilled-ceiling combined with desiccant cooling in hot and humid climates. *Energy and Buildings* **2002**, *34*, 487 – 495.

(15) Woods, J. Membrane processes for heating, ventilation, and air conditioning. *Renewable and Sustainable Energy Reviews* **2014**, *33*, 290–304.

(16) Zhang, L.-Z. Progress on heat and moisture recovery with membranes: From fundamentals to engineering applications. *Energy Conversion and Management* **2012**, *63*, 173 – 195, 10th International Conference on Sustainable Energy Technologies (SET 2011).

(17) Yang, B.; Yuan, W.; Gao, F.; Guo, B. A review of membrane-based air dehumidification. *Indoor and Built Environment* **2015**, *24*, 11–26.

(18) Zhang, L.-Z.; Wang, Y.-Y.; Wang, C.-L.; Xiang, H. Synthesis and characterization of a PVA/LiCl blend membrane for air dehumidification. *Journal of Membrane Science* **2008**, *308*, 198 – 206.

(19) Bui, T. D.; Chen, F.; Nida, A.; Chua, K. J.; Ng, K. C. Experimental and modeling analysis of membrane-based air dehumidification. *Separation and Purification Technology* **2015**, *144*, 114–122.

(20) Bui, D. T.; Nida, A.; Ng, K. C.; Chua, K. J. Water vapor permeation and dehumidification performance of poly (vinyl alcohol)/lithium chloride composite membranes. *Journal of Membrane Science* **2016**, *498*, 254–262.

(21) Ge, G.; Xiao, F.; Xu, X. Model-based optimal control of a dedicated outdoor air-chilled ceiling system using liquid desiccant and membrane-based total heat recovery. *Applied Energy* **2011**, *88*, 4180 – 4190.

(22) Xiao, F.; Ge, G.; Niu, X. Control performance of a dedicated outdoor air system adopting liquid desiccant dehumidification. *Applied Energy* **2011**, *88*, 143 – 149.

(23) Huang, S.-M.; Zhang, L.-Z. Researches and trends in membrane-based liquid desiccant air dehumidification. *Renewable and Sustainable Energy Reviews* **2013**, *28*, 425 – 440.

(24) Abdel-Salam, M. R.; Fauchoux, M.; Ge, G.; Besant, R. W.; Simonson, C. J. Expected energy and economic benefits, and environmental impacts for liquid-to-air membrane energy exchangers (LAMEEs) in HVAC systems: A review. *Applied Energy* **2014**, *127*, 202 – 218.

(25) Moghaddam, D. G.; Besant, R. W.; Simonson, C. J. Solution-side effectiveness for a

liquid-to-air membrane energy exchanger used as a dehumidifier/regenerator. *Applied Energy* **2014**, *113*, 872 – 882.

(26) Abdel-Salam, A. H.; Simonson, C. J. Annual evaluation of energy, environmental and economic performances of a membrane liquid desiccant air conditioning system with/without ERV. *Applied Energy* **2014**, *116*, 134 – 148.

(27) Das, R. S.; Jain, S. Performance characteristics of cross-flow membrane contactors for liquid desiccant systems. *Applied Energy* **2015**, *141*, 1 – 11.

(28) Zhang, N.; Yin, S.-Y.; Zhang, L.-Z. Performance study of a heat pump driven and hollow fiber membrane-based two-stage liquid desiccant air dehumidification system. *Applied Energy* **2016**, *179*, 727 – 737.

(29) Keniar, K.; Ghali, K.; Ghaddar, N. Study of solar regenerated membrane desiccant system to control humidity and decrease energy consumption in office spaces. *Applied Energy* **2015**, *138*, 121 – 132.

(30) Kumar, S.; Prevost, M.; Bugarel, R. Exergy analysis of a compression refrigeration system. *Heat Recovery Systems and CHP* **1989**, *9*, 151–157.

(31) Bayrakçi, H. C.; Özgür, A. E. Energy and exergy analysis of vapor compression refrigeration system using pure hydrocarbon refrigerants. *International journal of energy research* **2009**, *33*, 1070–1075.

(32) Ahamed, J.; Saidur, R.; Masjuki, H. A review on exergy analysis of vapor compression refrigeration system. *Renewable and Sustainable Energy Reviews* **2011**, *15*, 1593–1600.

(33) Zhang, L. Energy performance of independent air dehumidification systems with energy recovery measures. *Energy* **2006**, *31*, 1228 – 1242.

(34) Sakulpipatsin, P.; Itard, L.; van der Kooi, H.; Boelman, E.; Luscuere, P. An exergy application for analysis of buildings and HVAC systems. *Energy and Buildings* **2010**,

42, 90 – 99, International Conference on Building Energy and Environment (COBEE 2008).

(35) Qureshi, B. A.; Zubair, S. M. Application of exergy analysis to various psychrometric processes. *International Journal of Energy Research* **2003**, *27*, 1079–1094.

(36) Caliskan, H.; Hepbasli, A.; Dincer, I.; Maisotsenko, V. Thermodynamic performance assessment of a novel air cooling cycle: Maisotsenko cycle. *International Journal of Refrigeration* **2011**, *34*, 980 – 990.

(37) Mandegari, M. A.; Pahlavanzadeh, H.; Farzad, S. Energy approach analysis of desiccant wheel operation. *Energy Systems* **2014**, *5*, 551–569.

(38) Bynum, J. Thermodynamic modeling of a membrane dehumidification system. Ph.D. thesis, Texas A&M University, 2012.

(39) ASHRAE, *ANSI/ASHRAE Standard 62.1-2016: Ventilation for acceptable indoor air quality*; 2016.

(40) Mistry, K. H.; Lienhard, J. H. Generalized least energy of separation for desalination and other chemical separation processes. *Entropy* **2013**, *15*, 2046–2080.

(41) Bejan, A. *Advanced engineering thermodynamics*; John Wiley & Sons, 2016.

(42) Alhazmy, M. M. The minimum work required for air conditioning process. *Energy* **2006**, *31*, 2739–2749.

(43) McQuiston, F. C.; Parker, J. D.; Spitler, J. D. *Heating, ventilating, and air conditioning: Analysis and design*; John Wiley & Sons, 2005.

(44) Zhang, L.; Niu, J. Performance comparisons of desiccant wheels for air dehumidification and enthalpy recovery. *Applied Thermal Engineering* **2002**, *22*, 1347 – 1367.

(45) Zhang, L.-Z.; Fu, H.-X.; Yang, Q.-R.; Xu, J.-C. Performance comparisons of honeycomb-type adsorbent beds (wheels) for air dehumidification with various desiccant wall materials. *Energy* **2014**, *65*, 430 – 440.

(46) Fu, H.-X.; Yang, Q.-R.; Zhang, L.-Z. Effects of material properties on heat and mass transfer in honeycomb-type adsorbent wheels for total heat recovery. *Applied Thermal Engineering* **2017**, *118*, 345 – 356.

(47) Jurinak, J.; Mitchell, J.; Beckman, W. Open-cycle desiccant air conditioning as an alternative to vapor compression cooling in residential applications. *Journal of Solar Energy Engineering* **1984**, *106*, 253.

(48) Fu, H.-X.; Zhang, L.-Z.; Xu, J.-C.; Cai, R.-R. A dual-scale analysis of a desiccant wheel with a novel organic-inorganic hybrid adsorbent for energy recovery. *Applied Energy* **2016**, *163*, 167 – 179.

(49) Zhang, L.; Niu, J. Indoor humidity behaviors associated with decoupled cooling in hot and humid climates. *Building and Environment* **2003**, *38*, 99 – 107.

(50) De Antonellis, S.; Joppolo, C. M.; Molinaroli, L. Simulation, performance analysis and optimization of desiccant wheels. *Energy and Buildings* **2010**, *42*, 1386–1393.

(51) Zhang, X.; Dai, Y.; Wang, R. A simulation study of heat and mass transfer in a honeycombed rotary desiccant dehumidifier. *Applied Thermal Engineering* **2003**, *23*, 989–1003.

(52) De Antonellis, S.; Joppolo, C. M.; Molinaroli, L.; Pasini, A. Simulation and energy efficiency analysis of desiccant wheel systems for drying processes. *Energy* **2012**, *37*, 336–345.

(53) Duan, Z.; Zhan, C.; Zhang, X.; Mustafa, M.; Zhao, X.; Alimohammadisagvand, B.;

Hasan, A. Indirect evaporative cooling: Past, present and future potentials. *Renewable and Sustainable Energy Reviews* **2012**, *16*, 6823–6850.

(54) Elberling, L. Laboratory evaluation of the Coolerado Cooler indirect evaporative cooling unit. 2006.

(55) Angrisani, G.; Roselli, C.; Sasso, M. Effect of rotational speed on the performances of a desiccant wheel. *Applied Energy* **2013**, *104*, 268 – 275.

(56) Wang, N.; Zhang, J.; Xia, X. Desiccant wheel thermal performance modeling for indoor humidity optimal control. *Applied Energy* **2013**, *112*, 999 – 1005.

(57) Claridge, D. E.; Culp, C. H. Systems and methods for multi-stage air dehumidification and cooling. 2014; US Patent 8,641,806.

(58) Culp, C. H.; Claridge, D. E. Systems and methods for air dehumidification and sensible cooling using a multiple stage pump. 2013; US Patent 8,496,732.

(59) Claridge, D. E.; Culp, C. H. Systems and methods for air dehumidification and cooling with membrane water vapor rejection. 2013; US Patent 8,500,848.

Appendix: Details of desiccant model

In order to evaluate the maximum capacity of the desiccant dehumidifier, an equilibrium adsorption constant w_s is introduced to account for the maximum amount of water vapor adsorbed per unit mass of desiccant. Both Mandegari et al.[37] and De Antonellis et al.[50] discover that the equilibrium adsorption constant changes with inlet relative humidity ϕ by a power law as follows:

$$w_s = 0.24\phi^{2/3} \tag{27}$$

A desiccant wheel can be approximated as a cylinder; once the size and specific weight of the wheel is determined, the mass of the desiccant can be evaluated as follows:

$$m_{dec} = \epsilon\rho_{dw}\left(\frac{1}{2}\frac{3}{4}\pi R^2 L\right) \tag{28}$$

Here ϵ is the mass fraction of desiccant in the dehumidifier and R and L are radius and length of the desiccant wheel, respectively. Note that not all of the desiccant is working at the same time, as part of it is in the regeneration zone. A typical desiccant wheel has one fourth of the area for regeneration, and the rest under working conditions.[10,51] It is also assumed that at steady state, saturation lines are even distributed on the wheel, with the rotation starting at 0% and ending at 100% saturated. Therefore, only half of the working zone, on average, has the potential for adsorption.

Based on the two equations shown above, we can then determine the amount of water vapor separated from the stream. After multiplying the rotational speed N_{dw}, we can then calculate the outlet humidity ratio ω_2 as follows:

$$\Delta m_w = m_{w2} - m_{w1} = w_s \cdot m_{dec} = \frac{\dot{m}_a(\omega_2 - \omega_1)}{2\pi N_{dw}} \tag{29}$$

Zhang et al.[33,49] give a typical parametric setup for the silica gel desiccant wheel, where the size and operational condition of the wheel and properties of the desiccant are summa-

rized in Table 2.

Table 2: Parametric values of a typical setup for silica gel desiccant wheel.

Parameter and Property	Symbol	Value	Unit
Radius of the Wheel	R	20	cm
Length of the Wheel	L	20	cm
Density of the Wheel	ρ_{dw}	750	kg/m^3
Regeneration Temperature	T_{reg}	60	°C
Mass fraction of the Desiccant	ϵ	0.7	—